Electronic Supplementary Material (ESI) for ChemComm.

Supporting Information

Time-Resolved *In Situ* Powder X-ray Diffraction Reveals the Mechanisms of Molten Salt Synthesis

Saul J. Moorhouse, Yue Wu, Hannah C. Buckley and Dermot O'Hare

Contents

1 Experimental

All *in situ* XRD experiments were performed using the high-temperature configuration of ODISC on beamline I12 at the Diamond Light Source, UK.[1,2] In each case, stoichiometric quantities of starting material oxides Bi_2O_3, TiO_2, Fe_2O_3, and Cr_2O_3 were mixed with a seven-fold excess of the salt flux. For the monochromatic XRD experiments, Na_2SO_4 was chosen as the salt flux in preference to the K_2SO_4/Na_2SO_4 eutectic used in the previous EDXRD studies due to its well-defined melting point and to minimise the number of crystalline reflections from the flux. Results from *in situ* and *ex situ* experiments suggest that this change in molten salt had no effect on the mechanism or products of Aurivillius phase synthesis. The overall mass of the starting material mixture was greater than that used for laboratory studies to ensure the sample remained in the path of the X-ray beam throughout experimentation. Approximately 4 g of sample was loaded and packed down into an alumina crucible, which was positioned in a silicon carbide tube in the furnace. The mixtures were then heated to temperatures of up to 950 °C while XRD data was continually collected. Following cooling to room temperature, the structure of the product was established as a pure $n = 4$ Aurivillius phase, with $a = 5.464$ Å, $b = 5.435$ Å, $c = 40.997$ Å, and space group $A2_1am$. Characterisation of the symmetry-lowering transition on cooling is included in section 4. The lattice parameters are analogous to those of the end members of the $Bi_5Ti_3Fe_{1-x}Cr_xO_{15}$ series ($Bi_5Ti_3FeO_{15}$ reported by Hervoches *et al.*[3] and $Bi_5Ti_3CrO_{15}$ reported by Giddings *et al.*[4]), but with a *c*-parameter intermediate between the two.

EDXRD scans were recorded for 55 seconds at 60 second intervals. During angular-dispersive experimentation, images from the 2D detector were recorded with 4 second exposure at 30 second intervals. The energy of the monochromated beam was 83.5136 keV ($\lambda = 0.14846$ Å) and the detector was positioned 900.09 mm from the sample. The X-ray beam size for all data sets was 0.3 x 0.3 mm, which was applied using the positions of the entry slits. Diffraction scans were measured with 4 s exposure at 30 s intervals. In the case of angular-dispersive studies, the silicon carbide tube was raised within the furnace to a height above the X-ray beam path to eliminate peaks due to the crystalline tube. The temperature of the reacting mixture was accurately measured using a thermocouple positioned in contact with the powder sample. The 2D data were reduced using Fit2[5] and DAWN.[6] Refinements were performed using TOPAS academic V5.[7] Data below $2\theta = 0.90°$ and above $2\theta = 4.76°$ were cut due slight misalignments of the cell and of the beamstop, resulting in shadowing over part of the frames that would unevenly affect peak intensities.

2 Refinement details for *in situ* data

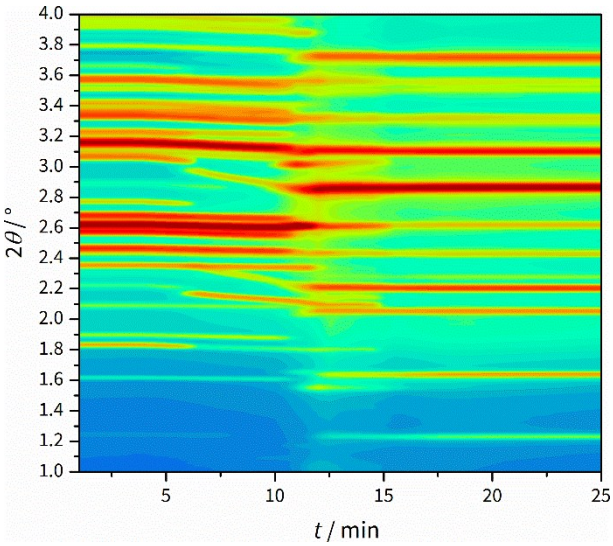

Figure 2.1. Heatmap of diffraction data for reaction **1**. The *β*- to *α*-Na_2SO_4 phase transition occurs at 6 min.

For reaction **1**, preliminary refinements were set up using data at various time points to confirm the presence of all relevant phases. No reaction was seen to occur before the *β*- to *α*-Na_2SO_4 phase transition (Figure 2.1), so this region was excluded from sequential refinements.

Multiphase sequential refinements were then performed in two sections due to the extremely large thermal expansion of the *α*-Na_2SO_4 phase. For data below 12 min, the sequential refinement was set up starting at 12 min going down, and each set of refined parameters was used as the starting parameters for the next refinement, down to 6 min. For data above 12 min, the refinement was run upward from 12 min to the end of the data set.

The refinement of data from reaction **2** was based on the refinement of **1**. However, the oscillating temperature profile resulted in some peaks moving in and out of overlap with one another (this is clearly visible in Figure 3 of the main text), affecting some phase intensities. Nevertheless, the overall conclusion drawn from this dataset does not change.

Data from reactions **3**-**5** were not analyzed using sequential refinement as the change in phase intensities was seen to not be representative of the reaction (most likely due to sample settling). In order to confirm phase assignments, however, Pawley models were refined against the data (provided in Q-space) converted into 2θ arbitrarily at λ = 0.1489 Å to provide a direct comparison to the ADXRD data (see Figure 4 of the main text). These models demonstrated clearly the major phases labelled in each example of EDXRD analysis.

3 Comparison of ADXRD and EDXRD

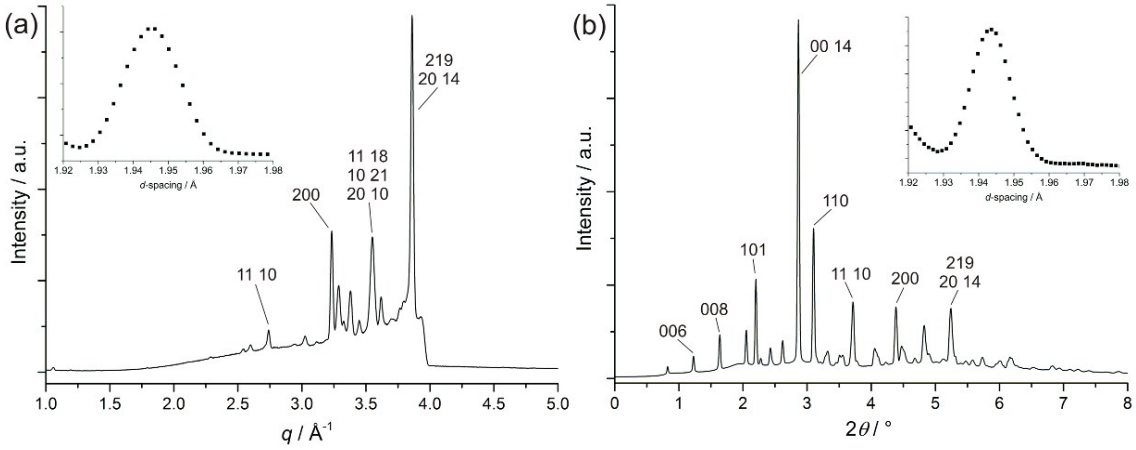

Figure 3.1. *In situ* XRD data for $Bi_5Ti_3Fe_{0.5}Cr_{0.5}O_{15}$ measured at 950 °C using ODISC. (a) A 55 second scan using EDXRD and (b) an angular-dispersive XRD scan with 4 second exposure. INSET FOR BOTH: the (200) product Bragg reflection plotted as a function of *d*-spacing.

The EDXRD technique is less appropriate for studying these systems in real time than angular-dispersive XRD. Because of the absorption edge due to the presence of bismuth, reflections above *ca.* q = 4.0 Å^{-1} (where $q = 2\pi/d$) are very low in intensity. Additionally, the fixed angle of the detector at 5° results in reflections at low q (high d-spacing) being excluded from the data. Consequently, high-quality XRD data could only be obtained over a small d-spacing range, *ca.* $1.5 \leq d$ / Å ≤ 3.2, using this technique. Fluorescence peaks due to the presence of bismuth in the reaction mixture were also observed in EDXRD data at the following energies: Kα_1 E = 77.12 keV (q = 3.38 Å^{-1}), Kα_2 E = 74.81 keV (q = 3.28 Å^{-1}) and Kβ_1 E = 87.34 keV (q = 3.83 Å^{-1}). One advantage of employing EDXRD was the ability to optimise the position of the gauge volume to exclude peaks due to the sample vessel.

A comparison of the data resolution from both techniques was undertaken using values for the full width at half maximum (FWHM) of the $Bi_5Ti_3Fe_{0.5}Cr_{0.5}O_{15}$ (200) Bragg reflection, inset in Figure 5.2. The values were obtained using a Gaussian fit to the data and are expressed in Ångstroms to enable comparison between the two data sets. The (200) FWHM for the EDXRD data was 0.019 Å, whereas that for the angular-dispersive data was significantly lower, at 0.013 Å. A smaller FWHM is indicative of better data resolution and this is the case for the angular-dispersive data, despite the *200* Bragg reflection being significantly broader than some reflections observed at lower 2ϑ. High-resolution data was particularly important for the identification of intermediates during synthesis of n = 4 Aurivillius phases. The large number of crystalline phases which exist prior to product formation, in addition to the similarity in position of many of the Bragg reflections of these phases, made their elucidation very challenging. Higher resolution data, available over a greater d-spacing range, made *in situ* studies using angular-dispersive diffraction more insightful.

4 Analysis of the $Bi_5Ti_3Fe_{0.5}Cr_{0.5}O_{15}$ high-temperature phase transition

Orthorhombic-tetragonal structure transitions at elevated temperatures have been reported in a number of Aurivillius phases.[3,8,9] A structure field map has been constructed for cation-doped analogues with even *n* to illustrate the relationship between Curie temperature, phase-transition temperature and the nature of the dopant.[10] Giddings and co-workers postulated the existence of a discontinuous phase transition of $Bi_5Ti_3CrO_{15}$ from the $A2_1am$ hettotype to the centrosymmetric $I4/mmm$ structure above 660 °C.[4] A similar transition was observed by Snedden *et al.* for the $Bi_5Ti_3FeO_{15}$ material at *ca.* 730 °C.[11] To investigate such a transition in $Bi_5Ti_3Fe_{0.5}Cr_{0.5}O_{15}$, cooling of the product from 950 °C was monitored, with emphasis on detecting growth of any reflections consistent with a structure of different symmetry to that observed in the sample at 950 °C.

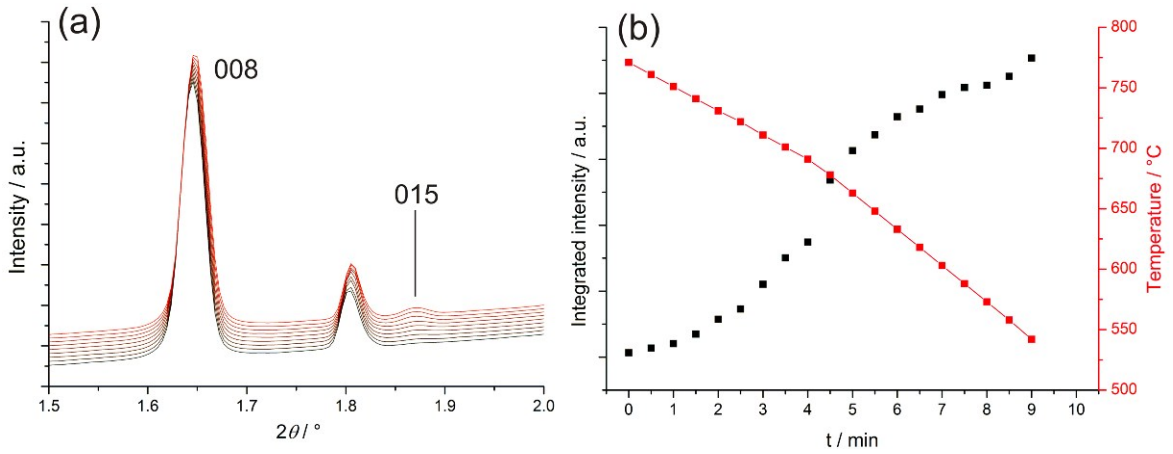

Figure 4.1. (a) Stack plot of *in situ* XRD data illustrating the growth of the (015) Bragg reflection upon sample cooling. Scans were recorded in the temperature range 731 °C (black) to 633 °C (red) in 10 °C increments (first five scans) and 15 °C increments (final four scans). (b) A plot of the change in integrated intensity of the (015) reflection (■) and sample temperature (■) as a function of time.

The use of angular-dispersive XRD was a necessity to study this phase transition. Observation of such low intensity Bragg reflections was not possible using EDXRD on Beamline I12 due to the lower data quality and restricted *d*-spacing range. The (015) reflection is not permitted by the $I4/mmm$ space group due to $k + l = 2n$ being forbidden, but is characteristic of $A2_1am$ symmetry. This reflection first appears on cooling in the scan recorded at 711 °C and steadily increases in intensity (Figure 4.1). The temperature at which this structural transition is observed is significant because it lies between known values for the Curie temperatures (and corresponding structural transitions) of the full Fe- and Cr-doped species.

Rietveld refinement analysis was undertaken using *in situ* data from selected scans recorded during product cooling. The lattice parameters elucidated from each refinement are plotted as a function of sample temperature in Figure 4.2. The unit cell volume of the low-temperature orthorhombic phase is approximately twice the size of the high-temperature tetragonal form and so $a_{orth} \sim b_{orth} = a_{tet}\sqrt{2}$.

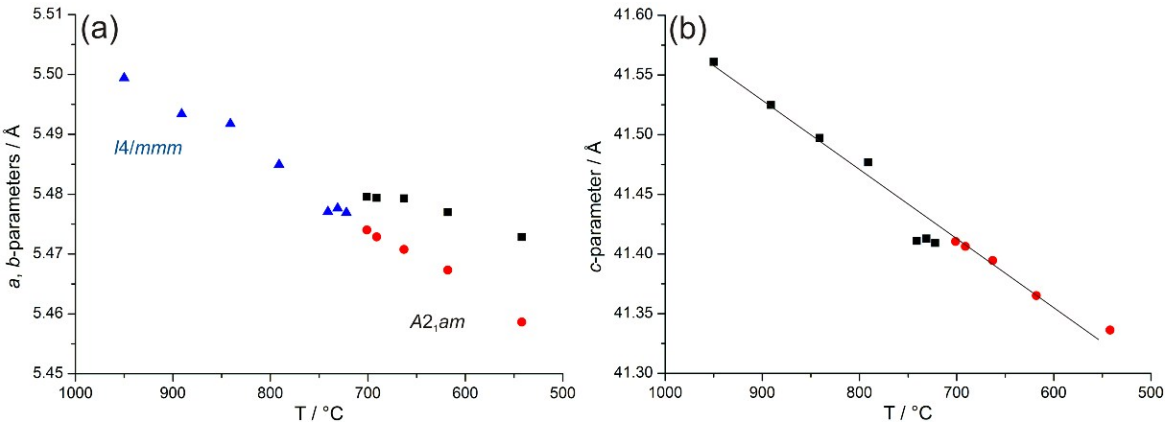

Figure 4.2. Thermal evolution of lattice parameters for $Bi_5Ti_3Fe_{0.5}Cr_{0.5}O_{15}$: (a) *a*- and *b*-parameters (where ▲ represents $a\sqrt{2}$ for *I*4/*mmm* symmetry, and ■ and ● represent *a* and *b* respectively for orthorhombic $A2_1am$ symmetry) and (b) *c*-parameter (where ■ represents *c* for *I*4/*mmm* symmetry, and ● represents *c* for orthorhombic $A2_1am$ symmetry). Lattice parameter error is within the data point.

A smooth trend in the lattice parameter variation with temperature is observed for the parent $Bi_5Ti_3FeO_{15}$ material throughout the orthorhombic-tetragonal phase transition. This is not the case for results from the $Bi_5Ti_3Fe_{0.5}Cr_{0.5}O_{15}$ material, which exhibit small discontinuities in *a*, *b,* and *c* at temperatures close to the observed structure change. This is perhaps suggestive of an indirect transition between the polar orthorhombic and centrosymmetric tetragonal structures, *via* an intermediate phase. Such behavior has been observed in similar Aurivillius compounds.[12] It would be particularly significant to observe an intermediate structure with *Amam* symmetry as such a phase was hypothesized, but could not be observed, for $Bi_5Ti_3CrO_{15}$. However, detection of such a short-lived intermediate structural variant requires further investigation to monitor precisely the existence of superlattice reflections throughout the entire temperature region of the phase change.

5 Further discussion of RbCl reaction

MSS of $Bi_5Ti_3FeO_{15}$ was attempted at three temperatures using RbCl. The XRD pattern from products synthesised at 800 °C contained reflections attributable to TiO_2, in addition to several other broad, low intensity reflections. Formation of the *n* = 4 phase was successful at 835 and 1000 °C. The stark contrast in observed product materials between 800 and 835 °C is highly indicative of a reaction 'barrier' somewhere in this temperature range. It appears that a different chemical feature of the system, rather than the melting of the salt at 718 °C, is required to be overcome before successful reaction can occur. The melting point of Bi_2O_3 is 824 °C.[2] It is highly possible that this physical change is the driving force towards *n* = 4 Aurivillius formation.

The reaction probed at 800 °C gives the strongest indication yet that the threshold to product formation in these systems is the melting of a Bi_2O_3-based phase. A crucial physical transformation appears to occur in the temperature region 815 ≤ T / °C ≤ 835. This observation is consistent with findings detailed in Section 4.5.2, where successful MSS with RbCl salt was observed following temperature dwell for 5 hours at 835 °C (above the Bi_2O_3 melting point of 824 °C) but not at 800 °C.

An increase in intensity of all Bragg reflections across the entire *q* range is observed in data measured shortly prior to and during the melting of the salt, at *ca.* 44 mins into the reaction. It is likely that this is a result of 'settling' of the sample in the path of the X-ray beam as the density of the salt changes upon melting. An increase in quantity of sample in the beam path correlates with a rise in Bragg reflection intensity. In addition to the growth in intensity of reflections due to crystalline phases, the 'background' due to scattering from amorphous materials in the beam path also varies significantly throughout sample heating and the melting of the salt. Diffraction due to scattering from non-crystalline phases was typically observed as a broad asymmetric signal in the data, which can be observed in the EDXRD scan shown in Figure 6 of the main text. This 'background' intensity was modelled using the method of Bruckner,[13] and then subtracted from the raw data. The subtracted intensity obtained following this analysis was plotted as a function of *q* and time, and the resulting contour plot is provided in Figure 5.1.

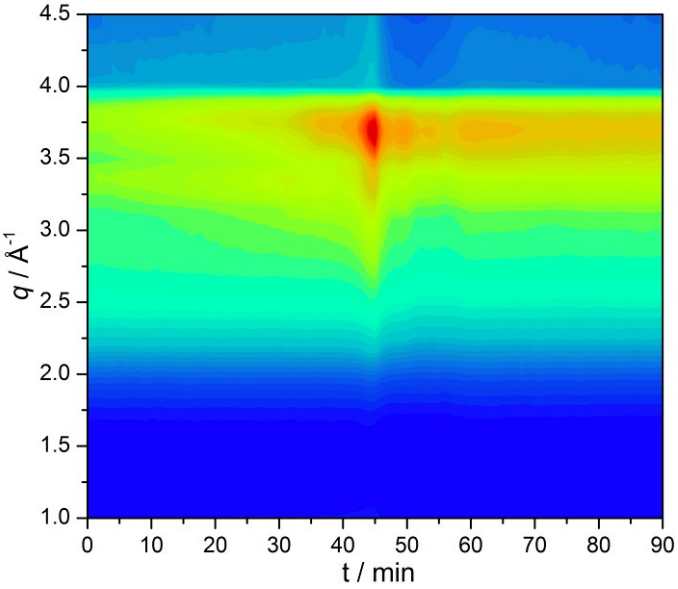

Figure 5.1. Contour plot containing the diffraction due to scattering from amorphous materials, extracted from raw *in situ* EDXRD data for the synthesis of $Bi_5Ti_3Fe_{0.5}Cr_{0.5}O_{15}$ with RbCl salt.

A maximum in the intensity of diffraction due to amorphous scattering coincides with the melting of the RbCl salt, which occurs after *ca.* 44 min. It is to be expected that such scattering should increase as the material in the X-ray beam transforms from the solid to the liquid phase, due to the decrease in long-range order of the sample. It is interesting to note that the scattering intensity is significantly greater during the melting transition than it is when RbCl exists purely in the liquid phase, at t > 50 min. It is possible that this coincides with additional melting of a Bi_2O_3-related species and the subsequent decay in the background is due to conversion of this material to the final crystalline product.

6 References

(1) Drakopoulos, M.; Connolley, T.; Reinhard, C.; Atwood, R.; Magdysyuk, O.; Vo, N.; Hart, M.; Connor, L.; Humphreys, B.; Howell, G.; Davies, S.; Hill, T.; Wilkin, G.; Pedersen, U.; Foster, A.; De Maio, N.; Basham, M.; Yuan, F.; Wanelik, K. *J. Synchrotron Radiat.* **2015**, *22* (Pt 3), 828.

(2) Moorhouse, S. J.; Vranješ, N.; Jupe, A.; Drakopoulos, M.; O'Hare, D. *Rev. Sci. Instrum.* **2012**, *83* (8), 84101.

(3) Hervoches, C. H.; Snedden, A.; Riggs, R.; Kilcoyne, S. H.; Manuel, P.; Lightfoot, P. *J. Solid State Chem.* **2002**, *164* (2), 280.

(4) Giddings, A. T.; Stennett, M. C.; Reid, D. P.; McCabe, E. E.; Greaves, C.; Hyatt, N. C. *J. Solid State Chem.* **2011**, *184* (2), 252.

(5) Hammersley, A. P. *FIT2D: An Introduction and Overview*; Report; 1997.

(6) Basham, M.; Filik, J.; Wharmby, M. T.; Chang, P. C. Y.; El Kassaby, B.; Gerring, M.; Aishima, J.; Levik, K.; Pulford, B. C. A.; Sikharulidze, I.; Sneddon, D.; Webber, M.; Dhesi, S. S.; Maccherozzi, F.; Svensson, O.; Brockhauser, S.; Náray, G.; Ashton, A. W. *J. Synchrotron Radiat.* **2015**, *22* (3), 853.

(7) Coelho, A. A. Coelho Software 2012,.

(8) Hervoches, C. H.; Lightfoot, P. *Chem. Mater.* **1999**, *11* (11), 3359.

(9) Krzhizhanovskaya, M.; Filatov, S.; Gusarov, V.; Paufler, P.; Bubnova, R.; Morozov, M.; Meyer, D. C. *Zeitschrift für Anorg. und Allg. Chemie* **2005**, *631* (9), 1603.

(10) Hyatt, N. C.; Reaney, I. M.; Knight, K. S. *Phys. Rev. B* **2005**, *71* (2), 24119.

(11) Snedden, A.; Hervoches, C. H.; Lightfoot, P. *Phys. Rev. B* **2003**, *67* (9), 92102.

(12) Srikanth, V.; Idink, H.; White, W. B.; Subbarao, E. C.; Rajagopal, H.; Sequeira, A. *Acta Crystallogr. Sect. B Struct. Sci.* **1996**, *52* (3), 432.

(13) Brückner, S. *J. Appl. Crystallogr.* **2000**, *33* (3), 977.